Function of the Pedicellate Spikelet and Awn in Sorghum and Related Grasses

Taylor AuBuchon-Elder[1a], Viktoriya Coneva[1,a,c], David M. Goad [a], Doug K. Allen[2,a,b,d], and Elizabeth A. Kellogg[2,a,d]

[a]Donald Danforth Plant Science Center, St. Louis, Missouri, 63132 USA
[b]USDA-ARS, St. Louis, Missouri, 63132 USA

[1]These authors contributed equally to this work.
[2]These authors contributed equally to this work.
[c]Current address: Kenyon College, Gambier, OH
[d]Address correspondence to: doug.allen@ars.usda.gov; ekellogg@danforthcenter.org

ORCID IDs: 0000-0002-0640-5135 (V.C.); 0000-0001-8658-6660 (D.M.G.); 0000-0001-8599-8946 (D.K.A.); 0000-0003-1671-7447 (E.A.K.)

Short title: Carbon assimilation in sorghum spikelets

The author responsible for distribution of materials integral to the findings presented in this article in accordance with the policy described in the Instructions for Authors (www.plantcell.org) is Elizabeth A. Kellogg (ekellogg@danforthcenter.org).

ABSTRACT

Sorghum and its relatives in the grass tribe Andropogoneae bear their flowers in pairs of spikelets. Seed is borne by the bisexual sessile spikelet, which sits directly on the inflorescence stem, while the other spikelet sits on a stalk (pedicel) and is sterile or staminate. Additionally, one floral bract (lemma) of the sessile spikelet often produces a long extension, the awn. The functions of the pedicellate spikelet and the awn are unknown. Pedicellate spikelets display extensive stomata on the surface of their enclosing bracts (glumes), whereas sessile spikelet glumes have few stomata, and the awn contains none. These observations suggest that pedicellate spikelets may be photosynthetic. We used radioactive and stable isotopes of carbon in pulse-chase and LC-MS/MS experiments, as well as RNA-seq of metabolically important enzymes to test the hypothesis that the pedicellate spikelet and awn provide photosynthate to the seed-bearing spikelet. Our results show that the pedicellate spikelet assimilates carbon into 4-carbon and Calvin cycle intermediates; carbon is translocated to the sessile spikelet, which is largely heterotrophic. The awn shows no evidence of photosynthesis. These results also apply to distantly related species of Andropogoneae. Finally, we show that removal of pedicellate spikelets in sorghum significantly reduces yield by ca. 5%, whereas the effect of awn removal is not significant. Thus, pedicellate spikelets affect yield in the cultivated species and most likely fitness in the wild ones.

INTRODUCTION

Sterile flowers or inflorescence structures are common among angiosperms. The plant effectively reduces potential reproductive output by taking floral structures "off line" to serve another purpose. Nonetheless this other function must increase plant fitness enough to compensate for removal of a meristem from the potential pool of flower- and seed-producing meristems. In other words, some meristems sacrifice their own seed making capacity to improve that of other meristems. In a few cases, the function of these sterile structures has been tested. For example, sterile flowers in some species help in pollinator attraction (e.g. (Jin et al., 2010; Morales et al., 2013)), and sterile inflorescences in Vitaceae form tendrils that anchor the vine (Boss and Thomas, 2002; Sousa-Baena et al., 2018).

The grain and bioenergy crop sorghum also produces sterile flowers in the inflorescence. The seed of sorghum, like that of many grasses, is enclosed in a set of floral bracts (glumes and lemmas), which together form a terminal unit known as a spikelet (a little spike)(Kellogg, 2015). The seed-bearing, or sessile (from the Latin verb meaning *to sit*), spikelet sits directly on the inflorescence axis. It is accompanied by an additional spikelet on a short stalk (pedicel); this is the pedicellate spikelet. The sessile and pedicellate spikelet together are known as a spikelet pair (Figure 1). Unlike the seed-bearing sessile spikelets, which are bisexual, the pedicellate spikelets are most commonly sterile in sorghum, although in some lines they produce stamens. Presence of a pedicellate spikelet, its shape, size and sex expression appear to be genetically fixed among plants of any given accession.

The function of the pedicellate spikelet is unknown. Because sorghum is wind-pollinated, the sterile spikelet cannot be involved in pollinator attraction so must have another function. One hypothesis is that the pedicellate spikelet is simply vestigial, an evolutionary relic that is gradually being eliminated by human selection. The ancestors of sorghum, and indeed almost all its relatives in the tribe Andropogoneae, also bear spikelet pairs and the pedicellate spikelets are also sterile or staminate (Kellogg, 2015). In these wild species, the pedicellate spikelet may function in seed dispersal and/or in controlling pollen to ovule ratio. However, the dispersal

function is not relevant in cultivated sorghum, in which the grains are not shed, and the pollen-producing function is only relevant in a minority of accessions.

Further complicating sorghum anatomy, the spikelet pair in sorghum also may include an awn on the sessile (seed-bearing) spikelet (Figure 1). The awn, when present, is a slender extension of the lemma (floral bract) of the upper flower, and may be twisted or nearly straight, and/or geniculate. Like the pedicellate spikelet, the presence, shape and size of the awn appears to be genetically fixed within an accession and its function has not been demonstrated in sorghum. In wild species of Andropogoneae in which the awn is twisted and geniculate, it is hygroscopic and can help orient the spikelet in the soil to enhance germination (Peart, 1979, 1981, 1984; Peart and Clifford, 1987). Awns have also been investigated extensively in wheat and rice as contributors to the carbon economy of the plant (Li et al., 2006)). Wheat and rice awns are vascularized and assimilate carbon, which is then transferred to the grain (Grundbacher, 1963; Motzo and Giunta, 2002; Li et al., 2006). However, neither the dispersal function nor the carbon assimilation function has been assessed in the sorghum awn.

It is possible that the pedicellate spikelet, the awn, or both produce photosynthate that contributes to grain filling. The spikelet is green, which suggests that it could be photosynthetically active, but its tiny size (3-6 mm) makes it unclear whether it could assimilate and export significant carbon to contribute to the carbon economy of other floral organs. In contrast, the awn is brown even soon after heading, suggesting that it might have limited capacity for photosynthesis. If so, its function must differ from that of the wheat or rice awn. The awn is also small, and in most sorghum lines, missing entirely.

Here we test the novel hypothesis that the pedicellate spikelet contributes photosynthate to the developing seed in sorghum, in a manner analogous to the awn in wheat or rice. In addition, we examine whether the awn also contributes to yield. We report a combination of spikelet removal, radioactive and stable carbon isotopic labeling and metabolite analyses, RNA seq experiments, and morphological observations with scanning electron microscopy (SEM). Through experiments with other members of the tribe Andropogoneae, our results are generalizable to the tribe. Finally, we conclude with a discussion of the adaptive value of these

structures in evolution, and their potential contribution to yield of an important drought-tolerant crop.

RESULTS

Sessile spikelets and awns are carbon sinks, pedicellate spikelets are sources

We initially tested whether the two types of spikelets and the awn were able to assimilate carbon dioxide, using a pulse-chase experiment to assess ^{14}C uptake. Inflorescence branches were exposed to ^{14}C for one hour. The two spikelet types and awns were separated either before or after exposure to ^{14}C (detached vs. attached). Measurements were standardized by weight (disintegrations per minute per mg), and are presented as a percentage of the total counts in spikelets and awns (Figure 2A). Pedicellate spikelets accounted for a substantially greater percentage of $^{14}CO_2$ taken up than sessile spikelets or awns, with the latter being scarcely detectable. This was true whether the inflorescences were intact, or whether the spikelets and awns were detached and lying on the bottom of the flask, suggesting that relative carbon uptake by the individual structures was consistent regardless of the effects of transpiration.

Intact inflorescences were also subjected to a pulse-chase with one-hour pulse labeling followed by 24-hour chase period in air (i.e., no additional labeled carbon provided during the chase). The fraction of counts in the pedicellate spikelet was reduced and that of the sessile spikelet increased, indicating translocation of carbon from one structure to the other (Figure 2A). The fraction in the awn was also elevated but still quite small relative to the spikelets.

To determine whether our result was specific to sorghum or might apply generally to Andropogoneae, we repeated the experiment with the distantly related species *Themeda triandra* and *Andropogon schirensis*, which, like sorghum, have sessile and pedicellate spikelets, with an awn on the sessile spikelet (Figure S1). These two species represent different major clades of Andropogoneae, and diverged ca. 15 million years ago (Estep et al., 2014). The results were similar to those for sorghum: most of the ^{14}C appeared in the pedicellate spikelet after 1 hour of labeling, whether it was attached to the inflorescence or not, but after a 24–hour chase the

proportion of label in the pedicellate spikelet had decreased and that in the sessile spikelet had increased (Figure S2, S3). Awns were scarcely labeled even after 24 hours.

The surface morphology of each organ is consistent with what would be expected from the ^{14}C results. The outer bracts (glumes) of pedicellate spikelets have obvious stomata in sorghum (Figure 2B) as well as in the other two species (Figure S2B, S3B), and are similar in this respect to leaves. Sessile spikelets, in contrast, have many fewer stomata; stomata are entirely absent for much of the surface (Figure 2C, S2C, S3C), although a few can be found near the apex in sorghum and on the sides of the glumes in *Andropogon schirensis* (not shown). No stomata were found on the awns (Figure 2D, S2D, S3D). The SEM data combined with the ^{14}C data provided an initial indication that the pedicellate spikelet might contribute photosynthate to the sessile spikelet, whereas the awn may not.

Pedicellate spikelets produce isotopically labeled Calvin cycle intermediates, sessile spikelets and awns are heterotrophic

We reasoned that the pedicellate spikelets should produce metabolites characteristic of photosynthesis if they are indeed sources of carbon for the grain. To test this hypothesis, the fate of the assimilated carbon was examined by exposing intact inflorescences to $^{13}CO_2$ for 30s, 60s or 300s, and then assessing key metabolites using LC-MS/MS. Specifically, because sorghum is a C_4 plant, we expected to see the label appear first in aspartate or malate, and subsequently in Calvin cycle intermediates, UDPG (in the sucrose biosynthetic pathway), and ADPG (in the starch biosynthesis pathway). Conversely, we expected that the sessile spikelet and awn should be metabolically distinct.

The results were qualitatively similar to those of the ^{14}C experiments, with the pedicellate spikelet assimilating more carbon than either the sessile spikelet or awn. Principal component analysis (PCA; Figure 3) showed differences in labeling over time. The first principal component (PC1) accounted for over 87% of the variance, distinguishing between values for unlabeled metabolites (loading just below 0) and those for labeled metabolites (loading positively). Pedicellate spikelet, sessile spikelet and awns thus differed according to the incorporation of

isotope with time. By five minutes, metabolite labeling in the pedicellate spikelet was distinct from other samples along PC1, consistent with the greatest label enrichment in the pedicellate during that period of time (Figure 3). PCA of the individual isotopologues gave similar results to those generated from average labeling values (Figure S4A). Overall effects of organ, time, and organ with time were all significant (generally $p \leq 0.0001$ for most metabolites) (Table S1A). Values for the pedicellate spikelets were significantly different from those of either of the other two organs (Tables S1B, S1C), but the sessile spikelet and awn were not significantly different from each other. In addition the five minute time point was significantly different from the 30 or 60 second pulses but no measureable difference was observed between the early two time points (Tables S1B, S1C).

The fraction of most metabolites that remained unlabeled (M0) decreased significantly over time in the pedicellate spikelet, but not in the sessile spikelet or awn (Figure 4, Table S2), confirming the ability of the pedicellate spikelet to fix carbon. Triose phosphates (the three-carbon sugar phosphates phosphoglyceric acid and dihydroxyacetone phosphate), the immediate products of RuBisCO-based carbon assimilation, were rapidly labeled and as a result had the greatest drop in the fraction of unlabeled isotopologues with time (Figure 4). By the end of the pulse at 5 minutes, the unlabeled fraction of triose phosphates was less than 40% of the total pool in pedicellate spikelets. Pyruvate that is a product of glycolysis and several steps removed from the Calvin cycle was significantly labeled (unlabeled fraction drops) as were hexose phosphates (glucose-6-phosphate, UDP-glucose and ADP-glucose) used in sucrose and starch biosynthesis respectively.

C_4 metabolite labeling (malate and aspartate) was surprisingly non-significant, presumably because of the size of each pool, most of which is involved in non-C_4 aspects of cellular metabolism (i.e. aspartate and malate are a combination of spatially distinct cellular and subcellular pools that vary in involvement in carbon assimilation). To further consider the extent of C_4 metabolism, we analyzed the presence of intermediates associated with photorespiration and vein spacing that also indicate the robustness of the carbon concentrating mechanism. Though 2-phosphoglycolate, glyoxylate, and glycolate are all intermediates in photorespiration that can be monitored by MS, typically investigations of photosynthetic metabolism with

isotopes in plants do not reliably detect or report all three (Weissmann et al., 2016; Arrivault et al., 2017). In sorghum, we were able to see small peaks for 2-phosphoglycolate (2-PG) and in the pedicellate spikelet, 2-PG trended to more labeling with time (Figure S5). Such results should be judged with caution though, as low levels of photorespiration are known to occur in C_4 plants (Zelitch et al., 2009). However pedicellate spikelet veins are farther apart than in C_4 leaves but closer to each other than those in sessile spikelets or C_3 leaves (Figure S6), suggesting that photosynthesis in inflorescence structures may not be easily categorized as C_3 or C_4.

Average labeling in metabolites is summarized in a simplified network (Figure 5) indicating percent ^{13}C incorporation per carbon at 5 min in pedicellate spikelets, sessile spikelets, and awns in sorghum. Incorporation was significantly less for sessile spikelets and awns; levels were consistent with or slightly above natural abundance and did not increase significantly during the time course of the labeling experiment.

To test the generality of our results, we repeated the $^{13}CO_2$ experiments with *Themeda triandra*. As in sorghum, the PCA showed a clear distinction between the pedicellate spikelets vs. the sessile spikelet and awn. PC1 explained 66% of the variance and the overall pattern of the PCA and isotopologue labeling is similar to those in sorghum (Figure S7A), suggesting that the results may apply to many other members of Andropogoneae.

RNA-seq confirmed C_4 photosynthetic metabolism in leaves and pedicellate spikelets, but not sessile spikelets or awns

To determine if gene expression in the three organ types reflected the metabolite data, we compared transcriptomes for spikelets and awns to those for leaves. As expected, and consistent with previous results, leaves and sessile spikelets were strikingly different. A PCA of the transcript data separated the two structures along PC1 (Figure S8), whereas awns and pedicellate spikelets were separated most clearly along PC2. Qualitative inspection of the 100 genes loading most heavily on PC1 found that the axis largely distinguished autotrophic (-) from heterotrophic (+) metabolism. The pedicellate spikelet and awns were less distinct on this axis. Genes contributing to the second PC axis appeared to be involved in carbohydrate rearrangement

relative to other catabolic and anabolic metabolic functions. A heat map of the same data (Figure S9) found inverse patterns of gene expression, in which genes that were upregulated in leaves were down-regulated in sessile spikelets and vice versa. Awns and pedicellate spikelets were clearly distinct from the other two organs in the heat maps. Despite the lack of apparent metabolic activity in awns suggested by the carbon labeling experiments, a set of genes was distinctly upregulated in awns.

We generated heat maps for the subset of genes that specifically control the metabolites measured with ^{13}C, and classified these according to the metabolic process in which they participate (Figure 6). Consistent with PCA and the heatmap of all genes, the expression pattern in the leaf is distinct from that in the spikelets and awn. Notably, three genes that are only associated with autotrophic metabolism, RuBisCO, phosphoribulokinase, and sedoheptulose-1,7-bisphosphatase (S17BPase), were expressed highly in the leaf, but at lower levels in the pedicellate spikelet, and absent in sessile spikelet or awn. A similar trend was exhibited by fructose 1,6-bisphosphatase (F16BPase) which is involved in sucrose production in photosynthetic tissues. The low level of F16BPase expression in sessile spikelets and awns indicated a lack of autotrophic metabolism. Also, as F16PBase can play an important role in gluconeogenesis, the absence of F16BPase gene expression in these two organs further supports heterotrophic metabolism with sessile spikelets and awns receiving carbon (presumably sucrose) from other plant organs as indicated by the ^{14}C pulse-chase.

Genes specific to C_4 metabolism, including the copy of phosphoenolpyruvate carboxylase (PEPC) located on chromosome 1, NADP-dependent malate dehydrogenase (NADP-MDH) and NADP-dependent malic enzyme (NADP-ME) were highly expressed in the leaf, followed by pedicellate spikelets. One isoform of aspartate aminotransferase (ASPAT) was also highly expressed whereas phosphoenolpyruvate carboxykinase (PEPCK) was not detected, indicating that sorghum pedicellate spikelets are similar to sorghum leaves that do not contain an active PEPCK pathway (Wang et al., 2014; Döring et al., 2016). Aminotransferases such as alanine aminotransferase (ALAAT), or genes commonly associated with nitrogen interchange involving glutamate, glutamine, or asparagine metabolism were also not significantly differentially expressed (Figure 6).

We collected analogous data for *Themeda triandra* and found similar results. Because *Themeda triandra* spikelets are subtended by a large leaf-like bract (see below), spikelet gene expression was compared to the bract rather than to a foliage leaf. PCA of all the data clearly separated the awns from the other organs along the first principal axis (31% of variance); the three replicate bract samples were distinguished from the other organs on PC2 (Figure S10). Bracts and sessile spikelets had negatively correlated patterns of gene expression, whereas gene expression in pedicellate (staminate) spikelets was intermediate to the other two organs. Awns had a distinct set of upregulated genes that were not reflected in photosynthetic metabolism.

Focusing only on metabolite-specific genes resulted in a pattern similar to that of the complete set of differentially expressed genes (Figure S11). (Note that our accession of *T. triandra* is a tetraploid (Birari, 1980; Estep et al., 2014) and also lacks a reference genome, so the list of genes is longer than that in sorghum and includes more isoforms.) Genes related to photosynthesis are upregulated in bracts and down-regulated in sessile spikelets, whereas the situation is opposite for genes involved in starch and sucrose metabolism. The pedicellate spikelets bear some similarity to both bracts and sessile spikelets, whereas awns have a unique expression profile that could not be easily grouped with others.

Pedicellate spikelets contribute to seed weight in sorghum

To test the influence of pedicellate spikelet function on plant grain yield, individual pedicellate spikelets were removed from alternating panicle branches at anthesis. Two experiments were undertaken, one of which investigated eight different accessions (Figure S12) and removed only pedicellate spikelets. A second experiment investigated the five accessions with awns, and tested the effects of pedicellate spikelet removal, awn removal, or removal of both together.

Removal of pedicellate spikelets caused a significant 5.2% reduction in seed weight ($p=0.0197$) when data from both experiments were combined (Figure 7A). Considering only experiment 1, spikelet removal reduced weight in seven of the eight sorghum lines tested (Figure 7B), although the reduction was significant in only two of the eight lines. The mean seed weight was higher in

one line (PI597971) from which pedicellate spikelets were removed, however the increase was not significant (p=0.3232). This result is likely to be an artifact caused by unexpectedly low seed weight in the control (unaltered) plant leading to high variance in mean seed weight for branches with pedicellate spikelets left on. Within the experimental (altered) plant, seed weight was lower in branches with spikelets removed. Nonetheless, this aberrant set of data was included in subsequent analyses.

In experiment 2 alone, removal of the pedicellate spikelet also led to an overall reduction in seed weight but the effect size was smaller (ca. 5%) and did not reach significance (p=0.9284)(not shown). Removal of awns had a much smaller effect (ca. 1%) and was non-significant (p=0.6917). Variation between accessions and between pots was much higher in this experiment than the previous one, for unknown reasons, making it harder to detect significant differences although trends in the data were in the expected direction, with seed weight affected by removal of structures.

Bracts enhance carbon assimilation in wild species

Pairing sterile photosynthetic spikelets with seed-bearing ones appears to increase seed weight, suggesting that having a leaf in the inflorescence could also provide carbon for the developing seed. The two wild species investigated, *Themeda triandra* and *Andropogon schirensis*, do bear modified leaves in the upper part of the plant, much closer to the spikelets than the flag leaves of sorghum. Our ^{14}C pulse-chase experiments allowed us to test whether these played a role in carbon assimilation.

In *A. schirensis*, the modified leaf is reduced largely to a sheath, with only a short blade. As expected, this modified leaf assimilated ^{14}C, but the percentage of total counts was approximately the same in the pulse and chase, indicating little transfer of label from the leaf to the spikelets (Figure 8A). The leaf sheath bears stomata throughout (Figure 8B), as expected for a photosynthetic structure. We assessed ^{14}C in the peduncle (the internode between the leaf node and the lowermost inflorescence node), but found only a small amount of label in the segments next to the nodes and little label in the internode. The results suggest that the leaf was not a major source of photosynthate for the inflorescence within the timeframe and conditions of this

experiment (anthesis) and the increased ^{14}C in sessile spikelets during the chase was largely accounted for by the drop in pedicellate spikelet values.

In contrast, the bract of *Themeda triandra* is closely connected to the spikelets, separated by an internode of only 2-4.5 mm. The bract fixed a large percentage of the ^{14}C in the 1 hour pulse, and that percentage dropped considerably in the chase, leading to a corresponding increase in the amount in the sessile spikelet plus awn (Figure 8C). The epidermal pattern of the bract is leaf-like, with extensive stomata (Figure 8D) Results of ^{13}C assimilation were qualitatively similar to those for ^{14}C (Figure S4B), with uptake by the bract dwarfing that of the sessile and pedicellate spikelets. Thus adding a leaf-like structure close to the spikelets clearly can enhance carbon assimilation, over and above that provided by the pedicellate spikelets themselves leaving open the question of bract versus pedicellate spikelet contributions to the carbon economy of grains.

DISCUSSION

Vascular plants are comprised of multiple tissues and organs that can perform autotrophic, heterotrophic or a combination (i.e. mixotrophic) metabolism. Though leaves and roots are defined by autotrophic and heterotrophic metabolism respectively, flowers and inflorescences are known to photosynthesize as well and to contribute fixed carbon to their own metabolism (Bazzaz and Carlson, 1979; Vemmos and Goldwin, 1994; Antlfinger and Wendel, 1997; Aschan and Pfanz, 2003). By contributing to the overall carbon budget of the plant, reproductive structures can lower the cost of reproduction, often by an appreciable amount. Reproductive tissues of oilseeds, for example, are often green and have capacities to assimilate carbon or re-assimilate respired carbon (King et al., 1998; Furbank et al., 2004; Ruuska et al., 2004; Schwender et al., 2004; Goffman et al., 2005; Allen et al., 2009) and use photosynthetic light energy to enable ATP (Asokanthan et al., 1997; Rolletschek et al., 2005) or reductant (Browse and Slack, 1985; Asokanthan et al., 1997; Ruuska et al., 2004) production. Such studies have focused on the contribution of sunlight to metabolically demanding processes such as fatty acid biosynthesis that generate large amounts of CO_2; however studies on ears, awns, and glumes

suggest a similar contribution to overall yield of photosynthate in some cereals (Bort et al., 1996; Sanchez-Bragado et al., 2014).

Pedicellate, non-seed-bearing spikelets in sorghum are photosynthetic, and, more importantly, appear to export carbon to the sessile seed-bearing ones, ultimately contributing about 5% to yield (Figure 7). Thus, the pedicellate spikelets nourish not only themselves but also the adjacent sessile spikelets. This estimate is consistent with earlier reports that photosynthesis from the sorghum inflorescence may account for 6-18% of yield (Fischer and Wilson, 1971; Evans and Wardlaw, 1976), and can now attribute that contribution to yield to a particular component of the inflorescence. Labeling studies are commonly used to assess plant phenotype (Allen, 2016) and assessments with ^{14}C or ^{13}C described here indicate that the pedicellate spikelet can assimilate $^{14}CO_2$ whether attached or detached from other structures. $^{13}CO_2$ labeling experiments and expression data on metabolic enzymes also support autotrophic metabolism in the pedicellate spikelets, and are consistent with leaf-like epidermal morphology of the glumes, with stomata distributed over most of the surface.

In contrast, sessile spikelets in sorghum appear to be largely heterotrophic at anthesis. Carbon assimilation in the sessile spikelet is lower than that of the pedicellate spikelet, but still easily detected in ^{14}C pulse-chase experiments (Figure 2A). Stomata are much less common on the surface of the glumes than in pedicellate spikelets, although not entirely absent (Figure 2B, C). Metabolite and transcriptome data are consistent with largely heterotrophic metabolism, although labeling of metabolites with ^{13}C was much less than that in the pedicellate spikelet (Figures 3, 4, 5 Tables S1, S2). Genes encoding proteins involved in the dark reactions of photosynthesis were not detected in sessile spikelets, whereas genes involved in starch synthesis were transcribed (Figure 6).

No evidence of CO_2 assimilation was found in sorghum awns (Figure 2A). We hypothesized initially that awns in sorghum would bear some similarity to those in wheat, barley, and rice (e.g., (Li et al., 2006; Maydup et al., 2010) and provide photosynthate to the developing grain. Awns in wheat, barley and rice are large relative to other inflorescence components and are clearly green. However, many important grasses of the Andropogonae, including sorghum and

its wild relatives, have small awns that are only one component of a complicated anatomy that contains other green inflorescence structures. Awns in sorghum do not take up ^{13}C or ^{14}C, whether isolated or intact, and none of the metabolites were labeled (Figures 3, 4, 5). No stomata are present on the surface of the awn (Figure 2D). While the awns are transcriptionally active and exhibit distinct gene expression patterns (Figure 6), none of the genes of primary carbon metabolism (carbon reduction, glycolysis, or starch synthesis) are upregulated relative to pedicellate spikelets or leaves.

The results for sorghum can be generalized to other members of the tribe Andropogoneae, as shown by data on the unrelated species *Andropogon schirensis* and *Themeda triandra*. In both species, the sessile spikelet is bisexual as in sorghum, has a firm outer glume, and bears an awn. The pedicellate spikelet in these species is staminate (male). Based on the same lines of evidence as presented for sorghum, pedicellate spikelets in these species are photosynthetic and export carbon to the heterotrophic sessile spikelet at anthesis. The awns do not assimilate carbon and lack any evidence of carbon assimilation, although, as in sorghum, they produce awn-specific gene transcripts.

Because the structure of the spikelet pair is conserved among the majority of Andropogoneae (maize being an exception), we can infer that the function of the pedicellate spikelet as a nurse tissue has been fixed and maintained by natural selection. The proximity of pedicellate spikelets to individual seeds may enable delivery of photoassimilates during stress such as drought-induced reduction in transpiration, when transport from the leaves might be lower.

If having a small photosynthetic companion spikelet boosts fitness or yield, then placing a leaf-like structure in the inflorescence closer than the flag leaf would seem to be even more favorable. The bract in *Themeda triandra* appears to have such a function, assimilating considerably more carbon than the pedicellate spikelet and transferring that carbon to the sessile spikelet. Metabolically and anatomically it is leaf-like. The bract in *Andropogon schirensis* is also photosynthetically active, but appears to transfer little carbon to the developing inflorescence. This may be a function of distance of translocation within the short time frames of these experiments. While the distance from the flag leaf to the panicle in sorghum is generally at least

30 cm and often twice that distance, the corresponding distance in *A. schirensis* is 14-21 cm, and that in *Themeda triandra* is 2-4.5 mm.

Awns in Andropogoneae are derived independently from those in Triticeae or rice (Teisher et al., 2017), and differ in structure and, as shown here, in physiology. Sorghum and other Andropogoneae have flattened awns that are twisted, often geniculate, and mostly brown in color. The lemma is reduced to a tiny hyaline structure with minimal vascularization. This structure is consistent with the observation that the awn does not help provision the seed or support itself through photosynthesis. This is quite different from the structure of the awn in Triticeae and rice, which is straight, clearly vascularized and connected to a large leaf-like lemma.

Whether pedicellate spikelets use a fully developed C_4 pathway remains unclear. Labeling of C_4 metabolites (aspartate and malate) was detectable but the enrichment for malate in particular was not high in either sorghum or *Themeda* triandra, reflecting a large unlabeled pool of malate not immediately used in CO_2 assimilation. Relative expression of photosynthetic enzymes is higher in pedicellate spikelets than in sessile spikelets or awns, but is lower than in leaves or bracts, respectively (Figure 6, S11). Furthermore vein to vein distances in the pedicellate spikelets of sorghum are farther apart than in a leaf (Figure S6), but closer than in most C_3 species or in sessile spikelets, suggesting the possibility of a limited C_4 shuttle.

Altered vein density can indicate that carbon assimilation occurs differently (Langdale et al., 1988) and may imply photosynthetic operation is distinct in non-leaf tissues. However, prior studies in other reproductive organs with isotope discrimination, photosynthetic gas analyses and immunolocalization of RuBisCO/PEPC suggest that anatomical changes alone do not preclude pseudo-C_4 function. In comparisons of corn husks and leaves for example (Pengelly et al., 2011) isotope discrimination results were comparable between tissues possibly indicating that husks operated in a C_4-like capacity. In addition, observed differences in vein spacing did not lead to altered CO_2 compensation points when the provision of O_2 was varied. When we performed isotopic labeling with $^{13}CO_2$ we observed the presence of labeled 2-phosphoglycolate in pedicellate spikelets and also some unlabeled 2-phosphoglycolate in other organs; however these

results cannot be unambiguously interpreted as C_4 plant organs can perform some photorespiration and require these pathway genes. Furthermore, expression patterns for 2-phosphoglycolate phosphatase, an enzyme specific to the photorespiratory pathway was not significantly different between organs and probably suggests that any role for photorespiration is minor.

The goal of current studies was to determine whether the pedicellate spikelet was assimilating carbon and whether it might be translocated to the sessile spikelet. Determining the precise photosynthetic pathway will require a different investigation. Immunolocalization of RuBisCO and PEPC or extended gas analyses (Pengelly et al., 2011) in a chamber specialized for small tissues could resolve these issues.

In summary, pedicellate spikelets in sorghum can make a small but significant contribution to yield. This is accomplished by fixing carbon and translocating it to the sessile spikelet, which holds the developing seed. Awns, in contrast, are carbon sinks, with limited metabolic activity. These results reflect millions of years of evolution, over which the spikelet pair has been selected and conserved. The pedicellate spikelet may thus have contributed to fitness in natural populations and could be a useful target for sorghum improvement in agricultural settings.

METHODS

Plant material

Sorghum bicolor accessions BTx623 (PI 564163), SO85 (PI 534096), Jola Nandyal (PI 534021), SAP-170 (PI 597971), SAP-51 (PI 655995), SAP-15 (PI 656014), SAP-257 (PI 656099), Combine Hegari (PI 659691) were obtained via the USDA Germplasm Resource Information Network (GRIN). All except SO85 are members of the Sorghum Association Panel (Casa et al., 2008). BTx623 is the line from which the reference genome sequence was obtained (Paterson et al., 2009; McCormick et al., 2018). Additional experiments were conducted on *Themeda triandra* (PI 208197), and *Andropogon schirensis* (*Pasquet s.n.*).

The three species represent different major clades of Andropogoneae (Estep et al., 2014). In addition, they differ in inflorescence structure. In sorghum, the pedicellate spikelets are sterile, whereas in the other two species, the pedicellate spikelets are staminate. In *T. triandra*, the sessile spikelet is associated with two staminate, pedicellate spikelets and is subtended by two additional pairs of staminate spikelets for a total of six staminate spikelets per sessile bisexual spikelet (Figure S1). For the purposes of this experiment, all six were considered similar and were treated together. In addition, the set of spikelets in *T. triandra* is closely subtended and partially enclosed by a large bract. In *A. schirensis*, there is no bract but the uppermost leaf is reduced to a sheath and minimal blade. The distance between the node of the leaf and the inflorescence node is 14–21 cm. *S. bicolor* has no bracts or inflorescence-associated leaves. In all three species, only the sessile, seed-bearing spikelet bears an awn.

Pulse-chase experiments, ^{14}C

Labeling. To determine which structures assimilated and fixed CO_2, we traced the localization of ^{14}C in *Sorghum bicolor* SO85, *Themeda triandra*, and *Andropogon schirensis*. Plants were collected at anthesis in the greenhouse between 10 and 11 AM. Culms were cut with a razorblade and placed directly into tap water before being transferred to 250 ml Erlenmeyer flasks containing filter paper and 1 mL of water, with two flasks per species. One flask (A) contained one (*Themeda*, *Sorghum*) or two (*Andropogon*) intact inflorescences, and was used for the 24-hour pulse-chase experiments. The second flask (B) for each species held one or two intact inflorescences and was used for the 1-hour pulse experiment. Flask B also contained an additional inflorescence dissected into sessile spikelets, pedicellate spikelets, awns, and bracts or leaves, to determine ^{14}C assimilation without connection to the rest of the inflorescence. Each experiment used ca. 40-80 mg of tissue, which for *T. triandra* equated to approximately: 15 awns, 22 bracts, 16-20 sessile spikelets, and 40 staminate spikelets. For *A. schirensis* a similar amount of biomass required approximately 25 awns, 22 sessile spikelets, 30 staminate spikelets, or 1 to 2 leaves. For *S. bicolor* we used 2.5 cm of one leaf, ~6-8 sessile spikelets, ~30 staminate spikelets, and all available awns from one inflorescence.

A plastic tube containing 12.5 microcuries of ^{14}C sodium bicarbonate was placed in each flask and maintained in an upright position by attachment to a plastic rod. Flasks were capped with airtight septa closures and 1 mL 6 N H_2SO_4 was added directly to each plastic tube using a syringe, releasing a pulse of $^{14}CO_2$ into the flask. All samples were incubated for one hour in a growth chamber at ~350µE.

Processing. After one hour, all flasks were purged with air (30-60 sec) to remove the $^{14}CO_2$. The radioactive gas stream was captured in a reservoir containing 2L of 2N KOH. For Flask A for each species, the airtight septum and closure was replaced with a sponge top prior to incubation in the growth chamber under continuous illumination for the 24-hour chase period. The contents flask B were analyzed immediately. Detached awns, sessile and pedicellate spikelets, and leaves were separated, weighed, and transferred to tubes containing cold methanol:chloroform (7:3, v:v) and steel beads. Simultaneously, the intact inflorescence was dissected, and individual components treated identically to the detached samples. Tissues were homogenized at 30 cycles/second in a bead homogenizer for two 5-minute intervals and were stored at -20°C for 48 hours. After 24 hours, samples from flask A were dissected, weighed and processed in the same way and stored at -20C for 24 hours.

All samples were extracted sequentially. The first extraction was based on 1.5 mL 7:3 (v:v) methanol:chloroform that was used to homogenize and store tissues after labeling. 200 uL from the methanol:chloroform extract was then combined with 5 mL of scintillation fluid (HIONIC FLUOR, Perkin Elmer). The remaining extract was removed from the residual biomass and water (2 mL) was added. The biomass was bead homogenized as before, centrifuged, and 200 uL was combined with 5mL scintillation fluid. Residual biomass was then treated with tissue solubilizer (ScintiGest), incubated overnight at 60°C and prepared for scintillation identically to prior extracts. Scintillation counting in disintegrations per minute (DPM) was performed on a Beckman Coulter LS-6000TA Scintillation Counter and included recording ^{14}C photon emissions for five minutes. After background subtraction from a blank that contained identical amounts of solvent and scintillation cocktail, total radioactivity per amount of tissue was calculated by accounting for differences in volume and mass.

Analysis of ^{14}C data. The total ^{14}C assimilation (DPM/mg) for each organ was calculated by summing the counts from the three serial extractions and accounting for the total volumes of each extraction. Then the percent of label within awn, pedicellate and sessile spikelets was determined by calculating the fractional ^{14}C assimilation in each organ. Experiments were repeated three (*Sorghum*, *Themeda*) or four (*Andropogon*) times. Percent label for each organ was averaged across experiments, and means and standard errors plotted in MS Excel.

^{13}C labeling in planta

<u>*Labeling*</u>. ^{13}C isotopic labeling studies were carried out on inflorescences of *Themeda triandra* and *Sorghum bicolor* accession SO85. *Themeda* and *Sorghum* plants were grown in the greenhouse until anthesis. The intact inflorescence was placed in a deflated plastic bag (inflated volume ca. 2-3 liters). A 10 mL serological pipet was fed into the bag with its tip near the apex of the inflorescence. The other end of the pipet was connected by hose to a tank of synthetic air comprised of $^{13}CO_2/N_2/O_2$ at a ratio of: 0.033:78:21.967. For each timed treatment, the bag was rapidly inflated (~15 L/min), and then the flow of gas was decreased to approximately 2 L/min. Structures were labeled for 30, 60 or 300 seconds. The synthetic air pumped into the bag flowed from the release of the pipet at the tip along the inflorescence structures and exited the bag at the point where the bag opening was grasped around the culm. At the end of the labeling period the inflorescence was cut immediately and dropped in a large pool of liquid nitrogen in a Styrofoam box (22 x 33 x 15 cm) to quench metabolism. During labeling and quenching plant tissues were exposed to greenhouse light levels between 250-400 uE.

Processing. Frozen tissue was dissected in liquid nitrogen to separate sessile and pedicellate spikelets, awns, and bracts. All materials were then ground with liquid nitrogen in mortar and pestle, extracted with methanol:chloroform (7:3 v:v) and then through addition of water to segregate polar and non-polar phases as described previously (Ma et al., 2014; Ma et al., 2017). PIPES (12 nmol) was added to each sample as an internal standard.

<u>*LC-MS/MS.*</u> A QTRAP 6500 tandem mass spectrometer linked to two Shimadzu LC-20AD pumps working in coordination with a SIL-20AC/HT autosampler was used to assess and

quantify the isotopic labeling in intermediates of primary metabolism. Extract from ca. five percent of the total harvested sample was injected. Standards for metabolites were run separately to establish retention time and in some cases confirm identification of isomers. Separation on LC involved an ion pair method (Ma et al., 2017) with flowrate of 300 microliters/min and a binary gradient buffer combination with Buffer A: 11 mM acetic acid with 10 mM tributylamine as the ion pair and Buffer B: 100% methanol. The method differed from prior work as the ramp profile was shortened with 3 min equilibration at 5% B, 10 min ramp to 35% B, 2 min ramp to 95% B, hold for 3 min, return to 5% B within 2 min, and equilibrate there for 11 min resulting in a total run time of 31 min The source inlet temperature (550°C), curtain gas (35 psi) and auxiliary gases (both set to 60 psi) were chosen based on optimal peak response. Declustering potential, collision energy and collision exit potential for individual mass transition pairs of multiple reaction monitoring were based on prior work (Ma et al., 2014; Ma et al., 2017).

Analysis of mass spectrometry data. Peak areas for individual mass traces that represent a precursor-product ion combination were integrated using MultiQuant 3.0.2 and Analyst 1.6 (AB Sciex). The relative percent combination of isotopologues was calculated along with ^{13}C average labeling that is defined as ($\frac{1}{n}\sum_{i=0}^{n} m_i \; x \; i$) with n equal to the number of carbons and m_i defining the relative isotopologue abundance for each of the i isotopologues measured. Data were additionally compared through the decrease in unlabeled fraction of the metabolite pool, referred to as M0 in the text, with PCA and anova-based tests of statistical significance generated in R software, as presented in the text and figures.

Sorghum spikelet removal experiments

Removal of pedicellate spikelets. The impact on grain weight of removing pedicellate spikelets was tested in all eight accessions (genotypes) of *Sorghum bicolor*.

Three to five pots were prepared for each genotype, with each pot containing two plants, one of which had a subset of pedicellate spikelets removed (the treated plant, plant A) and the other of which remained intact (the untreated plant, plant B). When both plants reached anthesis, pedicellate spikelets were removed with forceps from alternating branches of the plant A, which thus had a mix of treated and untreated branches. By removing pedicellate spikelets from alternating branches, variation along the inflorescence was averaged out. The untreated branches

of plant A thus serve as an internal control, and plant B is an external control. Treated branches were marked. Plants were grown to maturity, the inflorescence removed and dried at 40°C for 4-5 days, and spikelets harvested. Seeds were removed from the glumes and floral bracts. At least fifty seeds were recorded per treatment per plant although usually many more were available.

Removal of pedicellate spikelets, awns, and pedicellate spikelets+awns. Five of the genotypes bear awns on the sessile spikelet. These were grown with four plants per pot, six pots per genotype, with treatments as pedicellate spikelets removed (plant A), awns removed (plant B), awns and pedicellate spikelets removed (Plant C), and untreated (plant D). As with the first experiment, structures were removed from about half the branches of the treated plants in an alternating pattern up the inflorescence. Plants were grown, harvested, and mean seed weight calculated as in the previous experiment.

Data analysis: Seeds for each treatment/genotype combination were spread on a flatbed Epson Perfection V550 scanner (300dpi resolution, greyscale), imaged and weighed. The resulting JPG files were converted to binary images using Fiji (Abramoff et al., 2004) and the Analyze Particles tool used to count the seeds in each image. Total seed weight was divided by the number of seeds to estimate individual seed weight. The statistical effect of pedicellate spikelet, awn, and pedicellate spikelet and/or awn removal on seed weight was assessed using a mixed effect linear model (*lmer* function in R packages *lme4* (Bates et al., 2014) and *lmerTest* (Kuznetsova et al., 2015), where genotype, pot, and experiment were specified as random effects. All data were visualized using *ggplot2* (Wickham, 2016).

Scanning electron microscopy (SEM)

Plant material was fixed in formalin:acetic acid:50% alcohol (FAA) for a minimum of 24 hours and then transferred to 50% ethanol. Material was then taken through a standard ethanol dehydration series (70,80,90,95,100,100,100% EtOH) with at least 24 hours per stage. Samples were dried in a SamDri-780 critical point drier at the Washington University Center for Cellular Imaging (WUCCI), coated with gold palladium, and imaged on a Zeiss Merlin Field Emission SEM at 5.0 kV. Photographs were adjusted for brightness, contrast, and input levels using Adobe Photoshop.

RNA-Seq

To complement ^{13}C mass spec measurements of metabolites, expression levels for genes controlling photosynthesis, sugar and starch metabolism were estimated with RNA-seq. As with the ^{13}C experiments, material of *Sorghum bicolor* and *Themeda triandra* was harvested at anthesis and immediately frozen in liquid nitrogen and dissected while frozen. For sorghum, mature leaves and inflorescences were harvested from three plants. Inflorescences were hand dissected into pedicellate spikelet, sessile spikelet, and awn samples. For *Themeda triandra*, inflorescences from three tillers from one individual were dissected into bract, pedicellate spikelet, sessile spikelet, and awn. All samples were ground to a fine powder using liquid nitrogen. To extract total RNA, ca. 100 mg of tissue was added to 1 mL TRIzol reagent (15596026, Thermo Fisher Scientific) and the samples were vortexed. Next, 0.2 mL of chloroform was added, the samples were shaken for 15 s and incubated at room temperature for 3 min followed by centrifugation at 13,000 g for 15 min at 4°C and the upper aqueous phase was removed and added to 0.5 mL of isopropanol. The sample was incubated on ice for 10 min and centrifuged as above to obtain a nucleic acid pellet. The pellet was washed in 70 % (v/v) ethanol, air-dried briefly, and dissolved in 100 µL DEPC-treated water. Total RNA was cleaned and concentrated using an RNeasy kit (74104, QIAGEN) including on-column DNase treatment (79254, QIAGEN). Total RNA was quantified with a Qubit RNA HS kit (Q32852, Thermo Fisher Scientific). At least one sample for each organ was run on a RNA Pico Bioanalyzer microfluidics chip (Agilent) to calculate RNA integrity numbers (RIN). All RIN were in the range 7.8 – 9.5. RNA sequencing (RNA-Seq) libraries were prepared using SENSE mRNA library prep kit V2 for Illumina (001.24, Lexogen) with 500 ng input for all samples except for the three *Themeda* awn samples (160, 420, and 350 ng, respectively). The protocol was adjusted to produce a mean insert size of ~413 bp. Each library was indexed uniquely and amplified by 12 cycles of PCR for all samples except for *Themeda* awn samples, which were amplified using 14 cycles. Final libraries were quantified using a Qubit DNA HS kit (Q32854, Thermo Fisher Scientific). Select libraries were also run on a High Sensitivity DNA Bioanalyzer microfluidic chip (Agilent) to confirm library size in the desired range (~400 bp). Libraries were pooled by organism, resulting in 2 pools of 12 libraries at ~0.8 nM per library (10 nM final pool concentration). These pools were sequenced using Illumina HiSeq4000 paired end (2 x 150 bp)

technology at Michigan State University Genomics facility (https://rtsf.natsci.msu.edu/genomics/sequencing-services/).

Data analysis. Reads for *S. bicolor* were trimmed using Trimmomatic (Bolger et al., 2014) and mapped to the sorghum reference genome (Phytozome, Sbicolor_454_v3.1.1). Using HISAT (Kim et al., 2015) and StringTie (Pertea et al., 2015), alignments were read and transcripts were assembled and merged. To create expression level analysis, Ballgown was used according to the Tuxedo suite (Trapnell et al., 2012; Frazee et al., 2015) with TPM (transcripts per kilobase per million) files for each sample as the final output. Enzyme Commission (EC) numbers of relevant metabolic enzymes were retrieved from the KEGG pathway database (https://www.genome.jp/kegg/kegg3a.html). Expression levels of genes encoding these enzymes for each species and tissue were then extracted from the full transcriptomes using custom python scripts (https://github.com/ekellogg-lab/pedicellate-spikelet-carbon).

Reads for *Themeda triandra* were downloaded and submitted to Trinity (Grabherr et al., 2011) for automated trimming, quality filtering, assembly, and expression quantification. CDS and peptides were extracted using transdecoder (Haas et al., 2013). Orthologs of the metabolic genes in sorghum were identified by using OrthoFinder (Emms and Kelly, 2015) on the longest isoform of peptide sequences from the sorghum and maize genomes, and the predicted *Themeda* peptides. If an orthogroup contained a sorghum metabolism gene as identified in the sorghum transcriptome analysis, the *Themeda* peptides in that group were blasted against the sorghum peptides. If the *Themeda* gene's best match was a sorghum metabolism gene it was considered that gene's ortholog. The list of *Themeda* metabolism genes generated from this approach was then used for downstream analyses.

All downstream analyses were performed in R (RCoreTeam, 2013). Raw TPM outputs were normalized for library size across all samples for *S. bicolor* and *T. triandra* using the *calcNormFactors* function in the *edgeR* package (Robinson et al., 2010) and filtered to remove transcripts with fewer than 1 normalized TPM in at least 3 samples, effectively discarding unexpressed transcripts. Next, library-normalized TPM were $\log_2$-transformed and Tukey tests were performed using the function *TukeyHSD* in conjunction with ANOVA (Analysis of Variance) to generate all possible pairwise organ comparisons for each transcript in our metabolically-relevant gene list. The p-values generated by this approach were additionally

corrected for multiple testing using *p.adjust* with method set to "BH" (Benemjamini-Hochberg). Expression heatmaps for transcripts with at least one significant pairwise organ comparison (BH-corrected p-value < 0.05) were plotted using *pheatmap* (Kolde, 2015) using the ward.D2 clustering option. Manually annotated pathway descriptions are based on the Kyoto Encyclopedia of Genes and Genome (KEGG) pathway and biochemical textbook descriptions supported by comparative organ expression profile data. In instances where an enzyme could not be unambiguously assigned to a pathway, TargetP (Emanuelsson et al., 2007), a protein localization prediction tool, was used to determine possible organellar targeting and to guide descriptions. A subset of C_4 genes were identified based on phylogenetic literature and comparative genomic analysis (Wang et al., 2009; Huang et al., 2017). Principal Component Analysis (PCA) of metabolically relevant transcripts was performed using the function *prcomp* with $\log_2$-transformed TPM values, and visualized with functions in the *ggplot2* package (Wickham, 2016).

Acknowledgements: This work was supported in part by NSF grant DEB-1457748 to EAK, and through USDA-ARS support to DKA. The Proteomics and Mass Spectrometry Core facility is acknowledged for technical assistance and mass spectral data was obtained on an instrument funded by NSF-MRI grant DBI-1427621.

Author contributions: Conceptualization, Methodology, Investigation, Writing – Original Draft, Visualization: TA, VC, DKA, EAK. Formal Analysis and Writing, Review & Editing: All authors. Supervision: EAK and DKA. Project Administration: EAK. Funding Acquisition: EAK.

Literature Cited

Allen, D.K. (2016) Quantifying plant phenotypes with isotopic labeling and metabolic flux analysis. Curr. Opin. Biotechnol. **37:** 45-52.

Allen, D.K., Ohlrogge, J.B., and Shachar-Hill, Y. (2009) The role of light in soybean seed filling metabolism. Plant J. **58:** 220-234.

Antlfinger, A., and Wendel, L. (1997) Reproductive effort and floral photosynthesis in *Spiranthes cernua* (Orchidaceae). Am. J. Bot. **84:** 769-780.

Arrivault, S., Obata, T., Szecowka, M., Mengin, V., Guenther, M., Hoehne, M., Fernie, A.R., and Stitt, M. (2017) Metabolite pools and carbon flow during C_4 photosynthesis in maize: $^{13}CO_2$ labeling kinetics and cell type fractionation. J. Exp. Bot. **68:** 283-298.

Aschan, G., and Pfanz, H. (2003) Non-foliar photosynthesis - a strategy of additional carbon acquistion. Flora **198:** 81-97.

Asokanthan, P.S., Johnson, R.W., Griffith, M., and Krol, M. (1997) The photosynthetic potential of Canola embryos. Physiol. Plant. **101:** 353-360.

Bates, D., Maechler, M., Bolker, B., and Walker, S. (2014) *lme4*: Linear mixed-effects models using Eigen and S4 R package version, 1: 1-23.

Bazzaz, F.A., and Carlson, R.W. (1979) Contribution to reproductive effort by photosynthesis of flowers and fruits. Nature **279:** 554-555.

Birari, S.P. (1980) Apomixis and sexuality in *Themeda* Forssk. at different ploidy levels (Gramineae). Genetica **54:** 133-139.

Bolger, A.M., Lohse, M., and Usadel, B. (2014) Trimmomatic: A flexible trimmer for Illumina sequence data. Bioinformatics **30:** 2114-2120.

Bort, J., Brown, R.H., and Araus, J.L. (1996) Refixation of respiratory CO_2 in the ears of C_3 cereals. J. Exp. Bot. **47:** 1567-1575.

Boss, P.K., and Thomas, M.R. (2002) Association of dwarfism and floral induction with a grape 'green revolution' mutation. Nature **416:** 847-850.

Browse, J., and Slack, C.R. (1985) Fatty-acid synthesis in plastids from maturing safflower and linseed cotyledons. Planta **166:** 74-80.

Casa, A.M., Pressoir, G., Brown, P.J., Mitchell, S.E., Rooney, W.L., Tuinstra, M.R., Franks, C.D., and Kresovich, S. (2008) Community resources and strategies for association mapping in Sorghum. Crop Sci. **48:** 30-40.

Döring, F., Streubel, M., Bräutigam, A., and Gowik, U. (2016) Most photorespiratory genes are preferentially expressed in the bundle sheath cells of the C_4 grass *Sorghum bicolor*. J. Exp. Bot. **67:** 3053-3064.

Emanuelsson, O., Brunak, S., von Heijne, G., and Nielsen, H. (2007) Locating proteins in the cell using TargetP, SignalP and related tools. Nat. Protoc. **2:** 953-971.

Emms, D.M., and Kelly, S. (2015) Orthofinder: Solving fundamental biases in whole genome comparisons dramatically improves orthogroup inference accuracy. Genome Biol **16:** 157.

Estep, M.C., McKain, M.R., Vela Diaz, D., Zhong, J., Hodge, J.G., Hodkinson, T.R., Layton, D.J., Malcomber, S.T., Pasquet, R., and Kellogg, E.A. (2014) Allopolyploidy, diversification, and the miocene grassland expansion. Proc. Natl. Acad. Sci. USA **111:** 15149-15154.

Evans, L.T., and Wardlaw, I.F. (1976) Aspects of the comparative physiology of grain yield in cereals. Adv. Agron. **28:** 301-359.

Fischer, K.S., and Wilson, G.L. (1971) Studies of grain production in *Sorghum vulgare*. Ii. Sites responsible for grain dry matter production during the post-anthesis period. Aust. J. Agric. Res. **22:** 39-47.

Frazee, A.C., Pertea, G., Jaffe, A.E., Langmead, B., Salzberg, S.L., and Leek, J.T. (2015) Ballgown bridges the gap between transcriptome assembly and expression analysis. Nat. Biotechnol. **33:** 243-246.

Furbank, R.T., White, R., Palta, J.A., and Turner, N.C. (2004) Internal recycling of respiratory CO_2 in pods of chickpea (*Cicer arietinum* L.): The role of pod wall, seed coat, and embryo. J. Exp. Bot. **55:** 1687-1696.

Goffman, F.D., Alonso, A.P., Schwender, J., Shachar-Hill, Y., and Ohlrogge, J.B. (2005) Light enables a very high efficiency of carbon storage in developing embryos of rapeseed. Plant Physiol. **138:** 2269-2279.

Grabherr, M.G., Haas, B.J., Yassour, M., Levin, J.Z., Thompson, D.A., Amit, I., Adiconis, X., Fan, L., Raychowdhury, R., Zeng, Q., Chen, Z., Mauceli, E., Hacohen, N.,

Gnirke, A., Rhind, N., di Palma, F., Birren, B.W., Nusbaum, C., Lindblad-Toh, K., Friedman, N., and Regev, A. (2011) Full-length transcriptome assembly from RNA-seq data without a reference genome. Nat. Biotechnol. **29:** 644-652.

Grundbacher, F.J. (1963) The physiological function of the cereal awn. Bot. Rev. **29:** 366-381.

Haas, B.J., Papanicolaou, A., Yassour, M., Grabherr, M., Blood, P.D., Bowden, J., Couger, M.B., Eccles, D., Li, B., Lieber, M., MacManes, M.D., Ott, M., Orvis, J., Pochet, N., Strozzi, F., Weeks, N., Westerman, R., William, T., Dewey, C.N., Henschel, R., LeDuc, R.D., Friedman, N., and Regev, A. (2013) De novo transcript sequence reconstruction from RNA-seq using the Trinity platform for reference generation and analysis. Nat. Protoc. **8:** 1494-1512.

Huang, P., Studer, A.J., Schnable, J.C., Kellogg, E.A., and Brutnell, T.P. (2017) Cross species selection scans identify components of C_4 photosynthesis in the grasses. J. Exp. Bot. **68:** 127-135.

Jin, B., Wang, L., Wang, J., Teng, N.J., He, X.D., Mu, X.J., and Wang, Y.L. (2010) The structure and roles of sterile flowers in *Viburnum macrocephalum* f. Keteleeri (Adoxaceae). Plant Biol. (Stuttg) **12:** 853-862.

Kellogg, E.A. (2015) Poaceae. Pp. 1-416. In **Kubitzki, K.**, ed. The Families and Genera of Vascular Plants. Springer.

Kim, D., Langmead, B., and Salzberg, S.L. (2015) Hisat: A fast spliced aligner with low memory requirements. Nat. Methods **12:** 357-360.

King, S.P., Badger, M.R., and Furbank, R.T. (1998) CO_2 refixation characteristics of developing Canola seeds and silique wall. Austr. J. Plant Physiol. **25:** 377-386.

Kolde, R. (2015) *pheatmap*: Pretty heamaps. R package version 1.0.2.

Kuznetsova , A., Christensen, R.H., Bavay , C., and Brockhoff , P.B. (2015) Automated mixed ANOVA modeling of sensory and consumer data. Food Qual. Prefer. **40:** 31-38.

Langdale, J.A., Zelitch, I., Miller, E., and Nelson, T. (1988) Cell position and light influence C_4 versus C_3 patterns of photosynthetic gene expression in maize. EMBO J. **7:** 3643-3651.

Li, X., Wang, H., Li, H., Zhang, L., Teng, N., Lin, Q., Wang, J., Kuang, T., Li, Z., Li, B., Zhang, A., and Lin, J. (2006) Awns play a dominant role in carbohydrate production during the grain-filling stages in wheat (*Triticum aestivum*). Physiol. Plant. **127:** 701-709.

Ma, F., Jazmin, L.J., Young, J.D., and Allen, D.K. (2014) Isotopically nonstationary ^{13}C flux analysis of changes in *Arabidopsis thaliana* leaf metabolism due to high light acclimation. Proc. Natl. Acad. Sci. USA **111:** 16967-16972.

Ma, F., Jazmin, L.J., Young, J.D., and Allen, D.K. (2017) Isotopically nonstationary metabolic flux analysis (INST-MFA) of photosynthesis and photorespiration in plants. Methods Mol. Biol. **1653:** 167-194.

Maydup, M.L., Antonietta, M., Guiamet, J.J., Graciano, C., López, J.R., and Tambussi, E.A. (2010) The contribution of ear photosynthesis to grain filling in bread wheat (*Triticum aestivum* L.). Field Crops Res. **119:** 48-58.

McCormick, R.F., Truong, S.K., Sreedasyam, A., Jenkins, J., Shu, S., Sims, D., Kennedy, M., Amirebrahimi, M., Weers, B.D., McKinley, B., Mattison, A., Morishige, D.T., Grimwood, J., Schmutz, J., and Mullet, J.E. (2018) The *Sorghum bicolor* reference genome: Improved assembly, gene annotations, a transcriptome atlas, and signatures of genome organization. Plant J. **93:** 338-354.

Morales, C.L., Traveset, A., and Harder, L.D. (2013) Sterile flowers increase pollinator attraction and promote female success in the Mediterranean herb *Leopoldia comosa*. Ann. Bot. **111:** 103-111.

Motzo, R., and Giunta, F. (2002) Awnedness affects grain yield and kernel weight in near-isogenic lines of durum wheat. Austr. J. Agric. Res. **53:** 1285-1293.

Paterson, A.H., Bowers, J.E., Bruggmann, R., Dubchak, I., Grimwood, J., Gundlach, H., Haberer, G., Hellsten, U., Mitros, T., Poliakov, A., Schmutz, J., Spannagl, M., Tang, H., Wang, X., Wicker, T., Bharti, A.K., Chapman, J., Feltus, F.A., Gowik, U., Grigoriev, I.V., Lyons, E., Maher, C.A., Martis, M., Narechania, A., Otillar, R.P., Penning, B.W., Salamov, A.A., Wang, Y., Zhang, L., Carpita, N.C., Freeling, M., Gingle, A.R., Hash, C.T., Keller, B., Klein, P., Kresovich, S., McCann, M.C., Ming, R., Peterson, D.G., Mehboob ur, R., Ware, D., Westhoff, P., Mayer, K.F.X., Messing, J., and Rokhsar, D.S. (2009) The *Sorghum bicolor* genome and the diversification of grasses. Nature **457:** 551-556.

Peart, M.H. (1979) Experiments on the biological significance of the morphology of seed-dispersal units in grasses. J. Ecol. **67:** 843-863.

Peart, M.H. (1981) Further experiments on the biological significance of the morphology of seed-dispersal units in grasses. J. Ecol. **69:** 425-436.

Peart, M.H. (1984) The effects of morphology, orientation and position of grass diaspores on seedling survival. J. Ecol. **72:** 437-453.

Peart, M.H., and Clifford, H.T. (1987) The influence of diaspore morphology and soil-surface properties on the distribution of grasses. J. Ecol. **75:** 569-576.

Pengelly, J.J., Kwasny, S., Bala, S., Evans, J.R., Voznesenskaya, E.V., Koteyeva, N.K., Edwards, G.E., Furbank, R.T., and von Caemmerer, S. (2011) Functional analysis of corn husk photosynthesis. Plant Physiol. **156:** 503-513.

Pertea, M., Pertea, G.M., Antonescu, C.M., Chang, T.C., Mendell, J.T., and Salzberg, S.L. (2015) *Stringtie* enables improved reconstruction of a transcriptome from RNA-seq reads. Nat. Biotechnol. **33:** 290-295.

R Core Team (2013) R: A language and environment for statistical computing. R Foundation for Statistical Computing, Vienna, Austria.

Robinson, M.D., McCarthy, D.J., and Smyth, G.K. (2010) edgeR: A bioconductor package for differential expression analysis of digital gene expression data. Bioinformatics **26:** 139-140.

Rolletschek, H., Radchuk, R., Klukas, C., Schreiber, F., Wobus, U., and Borisjuk, L. (2005) Evidence of a key role for photosynthetic oxygen release in oil storage in developing soybean seeds. New Phytol. **167:** 777-786.

Ruuska, S.A., Schwender, J., and Ohlrogge, J.B. (2004) The capacity of green oilseeds to utilize photosynthesis to drive biosynthetic processes. Plant Physiol. **136:** 2700-2709.

Sanchez-Bragado, R., Molero, G., Reynolds, M.P., and Araus, J.L. (2014) Relative contribution of shoot and ear photosynthesis to grain filling in wheat under good agronomical conditions assessed by differential organ delta^{13}C. J. Exp. Bot. **65:** 5401-5413.

Schwender, J., Goffman, F., Ohlrogge, J.B., and Shachar-Hill, Y. (2004) Rubisco without the Calvin cycle improves the carbon efficiency of developing green seeds. Nature **432:** 779-782.

Sousa-Baena, M.S., Lohmann, L.G., Hernandes-Lopes, J., and Sinha, N.R. (2018) The molecular control of tendril development in angiosperms. New Phytol **218:** 944-958.

Teisher, J.K., McKain, M.R., Schaal, B.A., and Kellogg, E.A. (2017) Polyphyly of Arundinoideae (Poaceae) and evolution of the twisted geniculate lemma awn. Ann. Bot. **120:** 725-738.

Trapnell, C., Roberts, A., Goff, L., Pertea, G., Kim, D., Kelley, D.R., Pimentel, H., Salzberg, S.L., Rinn, J.L., and Pachter, L. (2012) Differential gene and transcript expression analysis of RNA-seq experiments with Tophat and Cufflinks. Nat. Protoc, **7:** 562-578.

Vemmos, S.N., and Goldwin, G.K. (1994) The photosynthetic activity of Cox's Orange Pippin apple in relation to fruit setting. Ann. Bot. **73:** 385-391.

Wang, X., Gowik, U., Tang, H., Bowers, J.E., Westhoff, P., and Paterson, A.H. (2009) Comparative genomic analysis of C_4 photosynthetic pathway evolution in grasses. Genome Biol. **10:** R68.

Wang, Y., Brautigam, A., Weber, A.P., and Zhu, X.G. (2014) Three distinct biochemical subtypes of C_4 photosynthesis? A modelling analysis. J. Exp. Bot. **65:** 3567-3578.

Weissmann, S., Ma, F., Furuyama, K., Gierse, J., Berg, H., Shao, Y., Taniguchi, M., Allen, D.K., and Brutnell, T.P. (2016) Interactions of C_4 subtype metabolic activities and transport in maize are revealed through the characterization of DCT2 mutants. Plant Cell **28:** 466-484.

Wickham, H. (2016) *ggplot2*: Elegant graphics for data analysis. Springer Verlag, New York.

Zelitch, I., Schultes, N.P., Peterson, R.B., Brown, P., and Brutnell, T.P. (2009) High glycolate oxidase activity is required for survival of maize in normal air. Plant Physiol. **149:** 195-204.

FIGURE LEGENDS

Figure 1. Spikelet pair structure in sorghum. A. Illustration of two spikelet pairs, marked by dotted lines, plus a terminal spikelet, which is morphologically identical to a pedicellate spikelet. Each pair is composed of a sessile spikelet, which includes a bisexual flower and bears the seed, and a pedicellate spikelet, which may be either sterile (most commonly) or staminate. The sessile spikelet bears a twisted awn from the lemma (floral bract). B. Spikelet pair of sorghum accession SAP-15 (PI 656014). SS, sessile spikelet; PS, pedicellate spikelet. Scale bar = 1 mm.

Figure 2. *Sorghum bicolor.* A. ^{14}C results. Percent dpm for each organ after 1 hour exposure to ^{14}C with organs removed from the axis (detached), inflorescence intact (attached), or after 24-hour chase. Values are similar after 1 hour, whether organs are attached or lying on filter paper. Change after 24-hour chase suggests movement of ^{14}C from pedicellate to sessile spikelet. Awn is largely unlabeled. B. Abaxial epidermis of pedicellate spikelet showing rows of stomata (arrows) and bicellular microhairs (m). C. Abaxial epidermis of sessile spikelet showing no stomata, but bicellular microhairs (m) and silica bodies (sb). D. Awn showing no stomata or other epidermal structures, except for prickles on the margin. Scale = 50 µm; note that B and C are more highly magnified than D.

Figure 3. Principal components analysis of ^{13}C labeled metabolites in sorghum, average labeling. Values for awn and sessile spikelet are not significantly different at any time point, whereas, values for the pedicellate spikelet are significantly different from the other organs, with the greatest variation in labeling at 5 minutes (300 sec). Organs are distinguished by color, time points by shape. A, awn; SS, sessile spikelet; PS, pedicellate spikelet; 30, values at 30 sec of labeling; 60, values at 60 sec of labeling; 300, values at 300 sec of labeling.

Figure 4. ^{13}C labeling for individual metabolites at three time points. Fraction of metabolite unlabeled. ASP, aspartate; ADPG, ADP-glucose; F6P, fructose-6-phosphate; G6P, glucose-6-phosphate; MAL, malate; PGA, phosphoglycerate; P5P, pentose 5 phosphates; PYR, pyruvate; TP, triose phosphates; UDPG, UDP-glucose. Points are mean percentages, bars are standard deviations. Colors distinguish the three organs. Most label accumulation occurs in the pedicellate spikelet and can be seen at 300 seconds.

Figure 5. Illustration of the fate of labeled carbon in sorghum metabolic network, after 300 seconds of labeling, showing the presumed cellular localization of each compound. Numbers in brackets are values at 300 seconds for the pedicellate spikelet, sessile spikelet, and awn, respectively. Most label accumulates in the pedicellate spikelet, with values for the sessile spikelet and awn much lower. Abbreviations as in Figure 4.

Figure 6. Relative expression of genes encoding biosynthetic enzymes immediately responsible for producing the metabolites labeled with ^{13}C. Heat map shows $\log_2$ transformed expression values. Putative biosynthetic pathways indicated as NITROGEN, CALVIN, STARCH, SUCROSE, REV_GLYCOLYSIS (reverse glycolysis), AA (amino acid metabolism), OPPP (oxidative pentose phosphate pathway), ANAPLEROTIC and C4.

Figure 7. Average seed weight (mg) from inflorescences with pedicellate spikelets untouched (on) and removed (off). A. Combined results of both removal experiments, showing 5.2% reduction in average weight with spikelet removal ($p=0.0197$). B. Average seed weight for each accession in experiment 1. Representative spikelet pair for each accession shown in Figure S1. * = $p < 0.05$.

Figure 8. A, C. ^{14}C results including bract. Percent dpm for each organ after 1 hour exposure to ^{14}C with organs removed from the axis (detached), inflorescence intact (attached), or after 24-hour chase. After 1 hour, most counts are in the bract when organs are detached from the stem but in the pedicellate spikelet when they are attached. Change after 24-hour chase suggests movement of ^{14}C from pedicellate to sessile spikelet. Awns remain largely unlabeled. A. *Andropogon schirensis*. C. *Themeda triandra*. B, D. Abaxial epidermis of bract showing rows of stomata (arrows). B. *Andropogon schirensis*. D. *Themeda triandra*, also with prickles (p). Scale = 50 µm.

Figure S1. Spikelet pair and inflorescence structure in *Andropogon schirensis* (A, B, C), and *Themeda triandra* (D, E, F, G). A. Illustration of two spikelet pairs of *A. schirensis*, marked by dotted lines. Each pair is composed of a sessile spikelet, which includes a bisexual flower and

bears the seed, and a pedicellate spikelet, which is staminate. The sessile spikelet bears a twisted awn from the lemma (floral bract). B. Spikelet pair of *A. schirensis*. C. Inflorescence of *A. schirensis*, showing two branches, each bearing 9-10 spikelet pairs. D. Spikelet pair of *T. triandra*, showing the dark indurate sessile spikelet, with two greenish pedicellate spikelets behind. One of the pedicellate spikelets is terminal on the short branch, so the three spikelets represent a pair plus a terminal spikelet that is morphologically identical to the pedicellate spikelet. E. Illustration of inflorescence structure in *T. triandra*, with three spikelet pairs, marked by dotted lines, and a terminal spikelet that is morphologically identical to the pedicellate spikelet. Spikelets in the proximal two pairs are all staminate; the distal pair includes a seed-bearing sessile spikelet and a staminate pedicellate spikelet. The sessile spikelet bears a twisted awn from the lemma (floral bract). F. Proximal spikelet pairs of *T. triandra*. All four proximal spikelets are staminate. G. Inflorescence branch of *T. triandra*, showing the spikelet complex as in D and E, subtended by a leaf-like bract. ss, sessile spikelet; ps, pedicellate spikelet; sts, staminate sessile spikelet. Scale bars B, D, F = 1 mm; C = 1 cm; G = 5 mm.

Figure S2. *Andropogon schirensis*. A. ^{14}C results. Percent dpm for each organ after 1 hour exposure to ^{14}C with organs removed from the axis (detached), inflorescence intact (attached), or after 24-hour chase. Values are similar after 1 hour, whether organs are attached or lying on filter paper. Change after 24-hour chase suggests movement of ^{14}C from PS to SS. Awn is largely unlabeled. B. Abaxial epidermis of pedicellate spikelet showing rows of stomata (arrows), bicellular microhairs (m), and prickles (p). C. Abaxial epidermis of sessile spikelet showing no stomata, but silica bodies (sb). D. Awn showing no stomata, but sparse macrohairs. Scale = 50 µm; note that B and C are more highly magnified than D.

Figure S3. *Themeda triandra*. A. ^{14}C results. Percent dpm for each organ after 1 hour exposure to ^{14}C with organs removed from the axis (detached), inflorescence intact (attached), or after 24-hour chase. Values are similar after 1 hour, whether organs are attached or lying on filter paper. Change after 24-hour chase suggests movement of ^{14}C from pedicellate to sessile spikelet. Awn is largely unlabeled. B. Abaxial epidermis of pedicellate spikelet showing rows of stomata (arrows), bicellular microhairs (m), and prickles (p). C. Abaxial epidermis of sessile spikelet

showing no stomata, but large pits (pit) and macrohairs (mac). D. Awn showing no stomata, but long macrohairs. Scale = 50 µm; note that B and C are more highly magnified than D.

Figure S4. PCA of all isotopologues for ^{13}C experiment, showing similarity of results between species. Awn and sessile spikelet are not significantly different for most metabolites, whereas pedicellate spikelet is significantly different from the other two organs. Values at 30 and 60 seconds are not significantly different for most metabolites but 300 second time point is distinct. A. *Sorghum bicolor*. B. *Themeda triandra*.

Figure S5. Isotopologues of 2-phosphoglycolate over time. 2-PG is labeled only in the pedicellate spikelet by the 300 second time point.

Figure S6. Cross section of glumes of sorghum spikelets, showing vein spacing. A. Pedicellate spikelet. Veins (indicated by arrows) are separated by three to five mesophyll cells, generally more than in the leaf. B. Sessile spikelet. Veins are small and distantly separated. Abaxial side is largely made up of thick-walled cells with no vascularization. Scale = 20 µm.

Figure S7. *Themeda triandra*, PCA of ^{13}C labeled metabolites, average labeling. Organs are distinguished by color, time points by shape. Awn, awn; SS, sessile spikelet; PS, pedicellate spikelet; Bract, bract. 30, values at 30 sec of labeling; 60, values at 60 sec of labeling; 300, values at 300 sec of labeling. A. Spikelets and awn only. Values for awn and sessile spikelet are not significantly different at any time point, whereas values for the pedicellate spikelet are significantly different, with the greatest variation in labeling at 5 minutes (300 sec). B. Spikelets, awn, and bract. Values for awn, sessile spikelet and pedicellate spikelet the same as those in A. Awn and sessile spikelet are not significantly different at any time point, whereas values for the pedicellate spikelet are significantly different from awn and sessile spikelet, and bract different from the other three organs, with the greatest variation in labeling at 5 minutes (300 sec).

Figure S8. *Sorghum bicolor*, PCA of gene expression data, showing distinct sets of transcripts for each organ. Values for each replicate experiments are similar. SS, sessile spikelet; PS, pedicellate spikelet.

Figure S9. *Sorghum bicolor*, heat map of all differentially expressed genes, by organ. Colors indicate relative expression level of genes, normalized by $\log_2$. SS, sessile spikelet; PS, pedicellate spikelet

Figure S10. *Themeda triandra*, PCA of gene expression data, showing distinct sets of transcripts for each organ. Values for each replicate experiments are similar, albeit with some outliers. SS, sessile spikelet; PS, pedicellate spikelet.

Figure S11. *Themeda triandra*. Relative expression of genes encoding biosynthetic enzymes immediately responsible for producing the metabolites labeled with ^{13}C. Heat map shows $\log_2$ transformed expression values. Putative biosynthetic pathways indicated as in Figure 6. Genes are in the same orthogroups as those shown for sorghum in Figure 6. SS, sessile spikelet; PS, pedicellate spikelet.

Figure S12. Spikelet pairs from the eight accessions used for spikelet removal experiments. A. SAP-170 (PI 597971). B. BTx623 (PI 564163). C. Combine Hegari (PI 659691). D SAP-257 (656099). E. SAP-51 (655995). F. Jola Nandyal (534021). G. SAP-15 (656014), H. SO85 (PI 534096). Arrow indicates pedicellate spikelet. All spikelets to the same scale. Scale bar = 1 mm.

Figure 1.

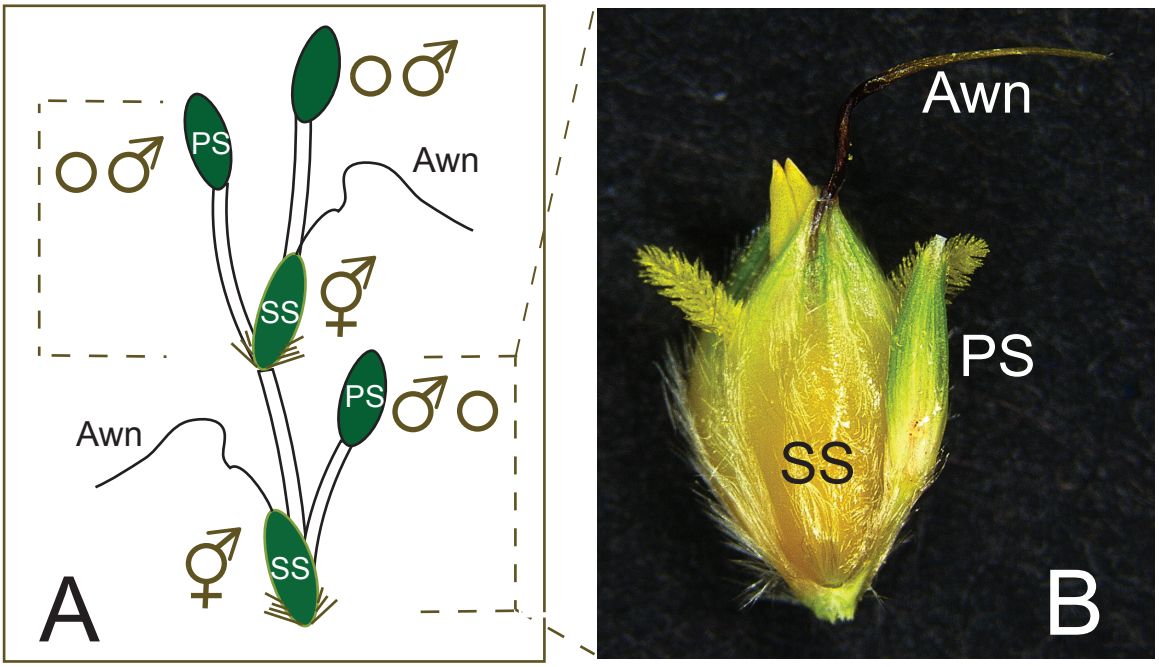

Figure 2.

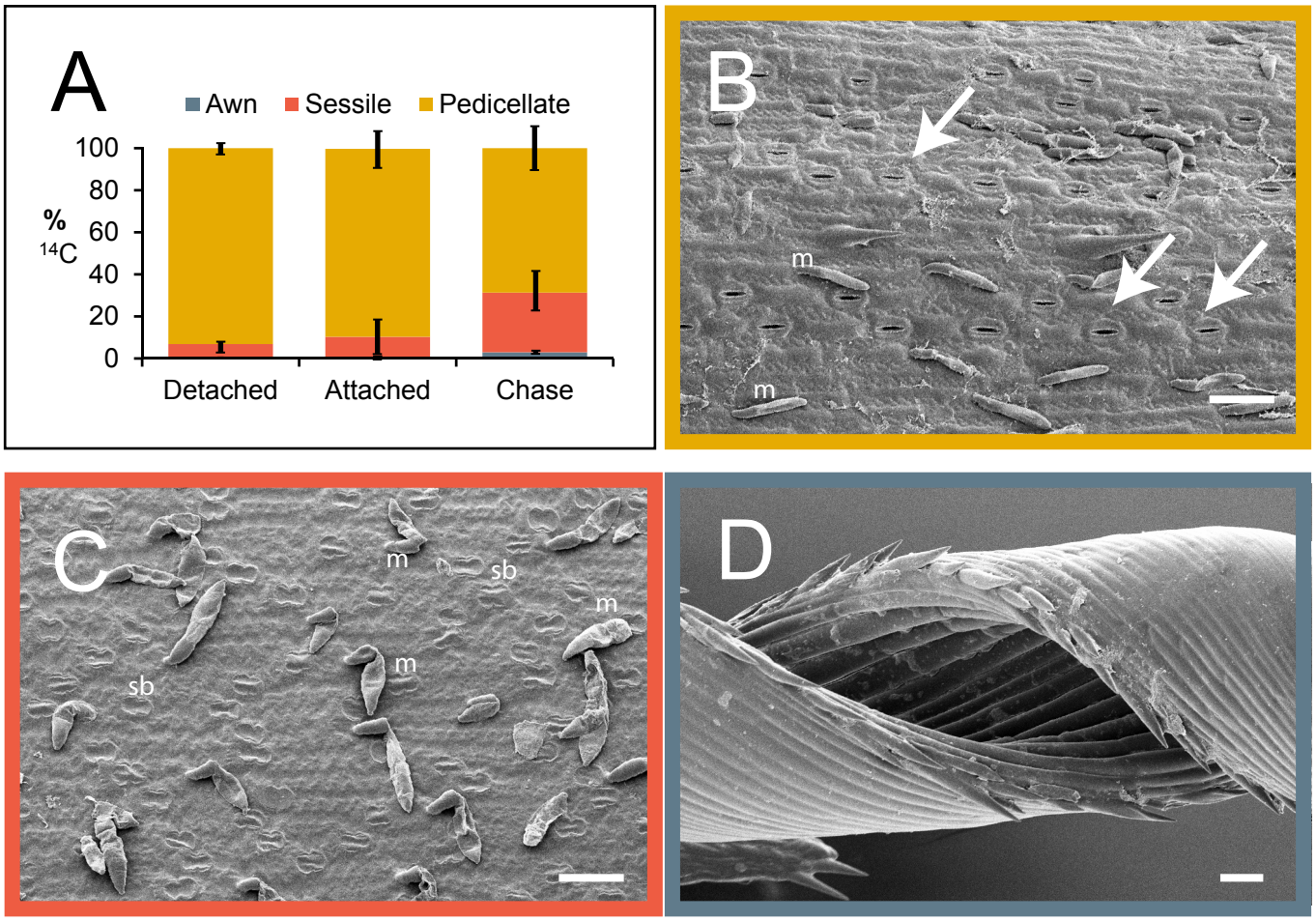
A
Awn
Sessile
Pedicellate
100
80
60
40
20
0
% ^{14}C
Detached
Attached
Chase
B
m
m
C
m
sb
m
m
sb
D

Figure 3.

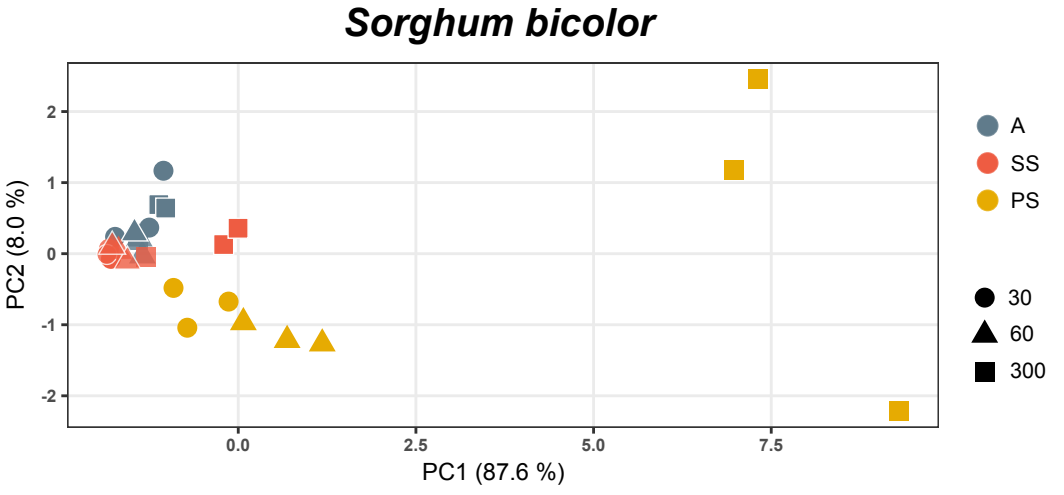
Sorghum bicolor
PC2 (8.0 %)
PC1 (87.6 %)
2
1
0
-1
-2
0.0
2.5
5.0
7.5
A
SS
PS
30
60
300

Figure 4.

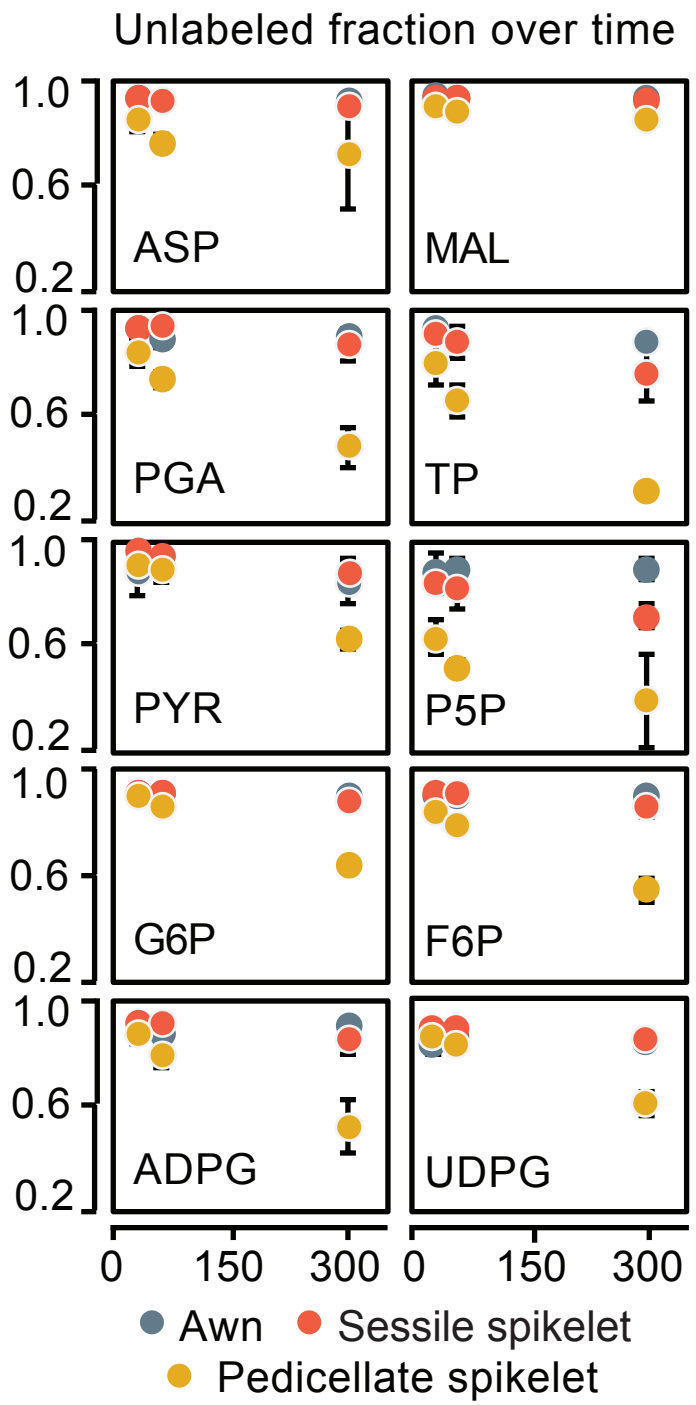
Unlabeled fraction over time
1.0
0.6
0.2
ASP
MAL
PGA
TP
PYR
P5P
G6P
F6P
ADPG
UDPG
0
150
300
Awn
Sessile spikelet
Pedicellate spikelet

Figure 5.

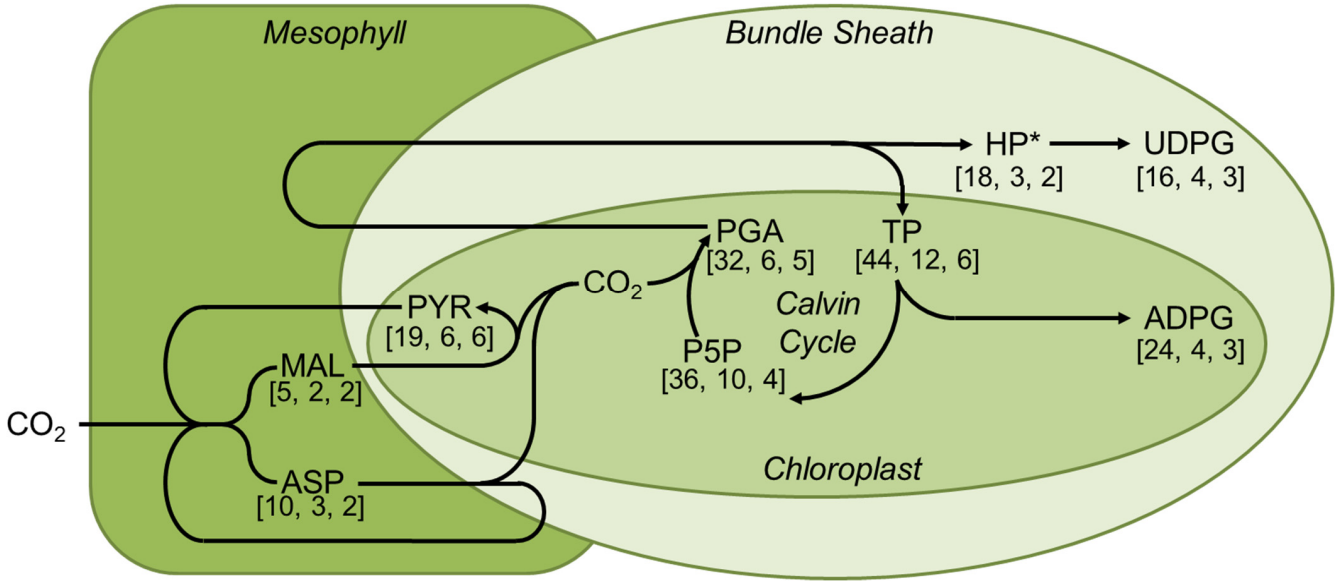
Mesophyll
Bundle Sheath
HP*
[18, 3, 2]
UDPG
[16, 4, 3]
PGA
[32, 6, 5]
TP
[44, 12, 6]
CO2
PYR
[19, 6, 6]
Calvin
Cycle
ADPG
[24, 4, 3]
P5P
[36, 10, 4]
MAL
[5, 2, 2]
CO2
ASP
[10, 3, 2]
Chloroplast

Figure 6.

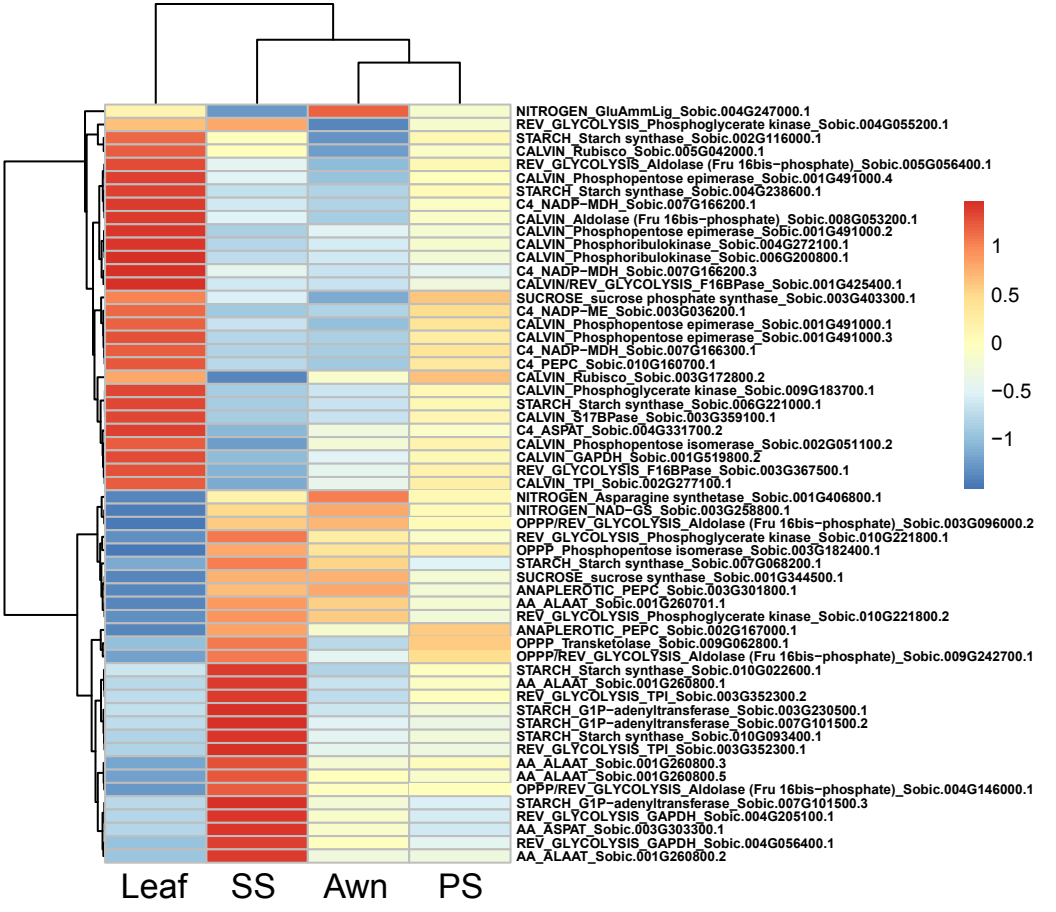
NITROGEN_GluAmmLig_Sobic.004G247000.1
REV_GLYCOLYSIS_Phosphoglycerate kinase_Sobic.004G055200.1
STARCH_Starch synthase_Sobic.002G116000.1
CALVIN_Rubisco_Sobic.005G042000.1
REV_GLYCOLYSIS_Aldolase (Fru 16bis−phosphate)_Sobic.005G056400.1
CALVIN_Phosphopentose epimerase_Sobic.001G491000.4
STARCH_Starch synthase_Sobic.004G238600.1
C4_NADP−MDH_Sobic.007G166200.1
CALVIN_Aldolase (Fru 16bis−phosphate)_Sobic.008G053200.1
CALVIN_Phosphopentose epimerase_Sobic.001G491000.2
CALVIN_Phosphoribulokinase_Sobic.004G272100.1
CALVIN_Phosphoribulokinase_Sobic.006G200800.1
C4_NADP−MDH_Sobic.007G166200.3
CALVIN/REV_GLYCOLYSIS_F16BPase_Sobic.001G425400.1
SUCROSE_sucrose phosphate synthase_Sobic.003G403300.1
C4_NADP−ME_Sobic.003G036200.1
CALVIN_Phosphopentose epimerase_Sobic.001G491000.1
CALVIN_Phosphopentose epimerase_Sobic.001G491000.3
C4_NADP−MDH_Sobic.007G166300.1
C4_PEPC_Sobic.010G160700.1
CALVIN_Rubisco_Sobic.003G172800.2
CALVIN_Phosphoglycerate kinase_Sobic.009G183700.1
STARCH_Starch synthase_Sobic.006G221000.1
CALVIN_S17BPase_Sobic.003G359100.1
C4_ASPAT_Sobic.004G331700.2
CALVIN_Phosphopentose isomerase_Sobic.002G051100.2
CALVIN_GAPDH_Sobic.001G519800.2
REV_GLYCOLYSIS_F16BPase_Sobic.003G367500.1
CALVIN_TPI_Sobic.002G277100.1
NITROGEN_Asparagine synthetase_Sobic.001G406800.1
NITROGEN_NAD−GS_Sobic.003G258800.1
OPPP/REV_GLYCOLYSIS_Aldolase (Fru 16bis−phosphate)_Sobic.003G096000.2
REV_GLYCOLYSIS_Phosphoglycerate kinase_Sobic.010G221800.1
OPPP_Phosphopentose isomerase_Sobic.003G182400.1
STARCH_Starch synthase_Sobic.007G068200.1
SUCROSE_sucrose synthase_Sobic.001G344500.1
ANAPLEROTIC_PEPC_Sobic.003G301800.1
AA_ALAAT_Sobic.001G260701.1
REV_GLYCOLYSIS_Phosphoglycerate kinase_Sobic.010G221800.2
ANAPLEROTIC_PEPC_Sobic.002G167000.1
OPPP_Transketolase_Sobic.009G062800.1
OPPP/REV_GLYCOLYSIS_Aldolase (Fru 16bis−phosphate)_Sobic.009G242700.1
STARCH_Starch synthase_Sobic.010G022600.1
AA_ALAAT_Sobic.001G260800.1
REV_GLYCOLYSIS_TPI_Sobic.003G352300.2
STARCH_G1P−adenyltransferase_Sobic.003G230500.1
STARCH_G1P−adenyltransferase_Sobic.007G101500.2
STARCH_Starch synthase_Sobic.010G093400.1
REV_GLYCOLYSIS_TPI_Sobic.003G352300.1
AA_ALAAT_Sobic.001G260800.3
AA_ALAAT_Sobic.001G260800.5
OPPP/REV_GLYCOLYSIS_Aldolase (Fru 16bis−phosphate)_Sobic.004G146000.1
STARCH_G1P−adenyltransferase_Sobic.007G101500.3
REV_GLYCOLYSIS_GAPDH_Sobic.004G205100.1
AA_ASPAT_Sobic.003G303300.1
REV_GLYCOLYSIS_GAPDH_Sobic.004G056400.1
AA_ALAAT_Sobic.001G260800.2
1
0.5
0
−0.5
−1
Leaf
SS
Awn
PS

Figure 7.

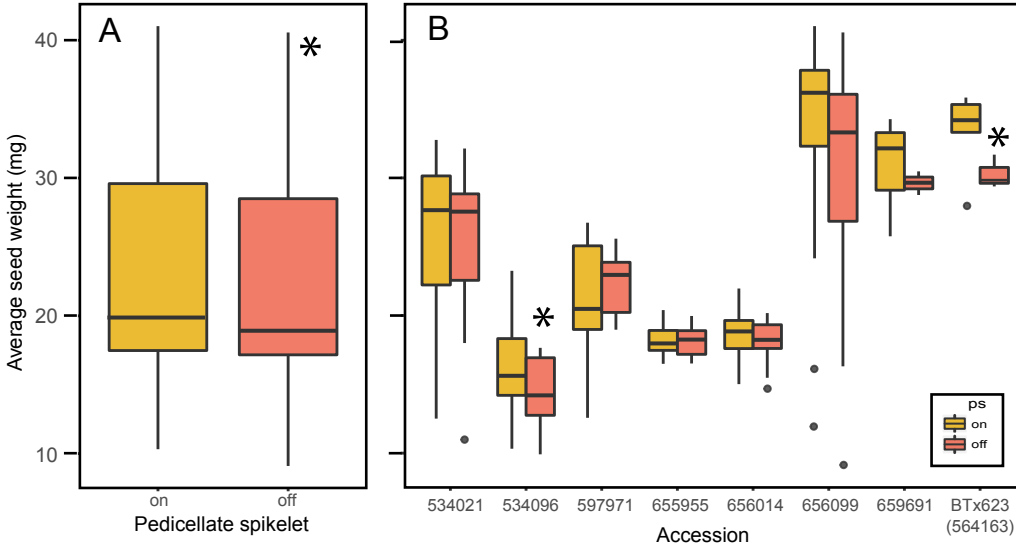
A
B
Average seed weight (mg)
40
30
20
10
*
*
*
on
off
Pedicellate spikelet
534021
534096
597971
655955
656014
656099
659691
BTx623
(564163)
Accession
ps
on
off

Figure 8.

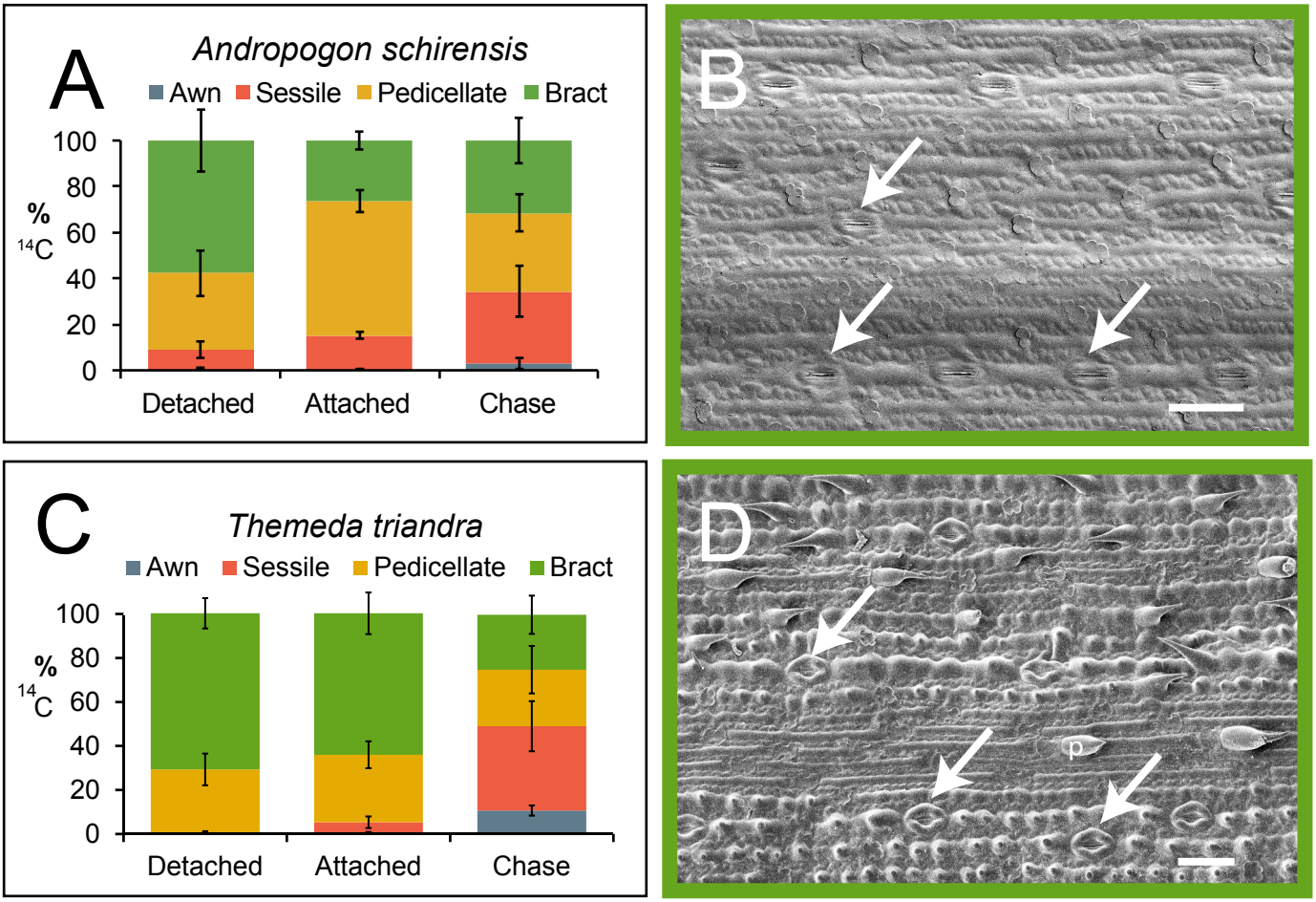
A
Andropogon schirensis
Awn
Sessile
Pedicellate
Bract
100
80
60
40
20
0
% 14C
Detached
Attached
Chase
B
C
Themeda triandra
Awn
Sessile
Pedicellate
Bract
100
80
60
40
20
0
% 14C
Detached
Attached
Chase
D
p